NASA TECHNICAL REPORT

NASA TR R-213

LOAN COPY: RETURN
AFWL (WLIL-2)
KIRTLAND AFB, N M

0067967

TECH LIBRARY KAFB, NM

NASA TR R-213

CORRELATION OF SONIC-BOOM THEORY WITH WIND-TUNNEL AND FLIGHT MEASUREMENTS

by Harry W. Carlson

Langley Research Center
Langley Station, Hampton, Va.

NATIONAL AERONAUTICS AND SPACE ADMINISTRATION • WASHINGTON, D. C. • DECEMBER 1964

TECH LIBRARY KAFB, NM
0067967

CORRELATION OF SONIC-BOOM THEORY WITH WIND-TUNNEL AND FLIGHT MEASUREMENTS

By Harry W. Carlson

Langley Research Center
Langley Station, Hampton, Va.

NATIONAL AERONAUTICS AND SPACE ADMINISTRATION

For sale by the Office of Technical Services, Department of Commerce,
Washington, D.C. 20230 -- Price $0.75

CORRELATION OF SONIC-BOOM THEORY WITH WIND-TUNNEL AND FLIGHT MEASUREMENTS

By Harry W. Carlson
Langley Research Center

SUMMARY

A study has been made of the accuracy and reliability of current theoretical methods of estimating sonic-boom overpressures for level flight at a constant supersonic Mach number. Theoretical estimation methods have been outlined and a numerical evaluation of sonic-boom theory for use on high-speed electronic computing machines has been introduced. Estimates based on this theory have been compared with available wind-tunnel and flight measurements. The correlation has been made with wind-tunnel data which incorporate improved data-reduction methods. The dependence of sonic-boom overpressure on configuration geometry has also been discussed and design methods of minimizing the problem have been explored. The results of this review have reaffirmed the conclusion that both volume and lift effects contribute to bow-shock overpressures. The results have also shown that existing theory provides reasonably accurate estimates of nominal ground-track overpressures for steady supersonic flight in a standard or near-standard atmosphere.

INTRODUCTION

The sonic boom, which only a decade ago was an interesting but little-recognized and little-understood physical phenomenon, has now emerged as a major concern in the operation of present military airplanes and poses one of the most serious operational problems to be encountered in the development of commercial supersonic transports. In recent years, intensive research efforts treating all phases of the problem have served to provide a basic understanding of this phenomenon. The theoretical studies of references 1 to 3 have resulted in the development of estimation methods which have been generally substantiated in correlations with the wind-tunnel data of references 4 to 7 and with the flight data of references 8 to 13. Effects of atmospheric nonuniformities and airplane acceleration and maneuvers have been treated theoretically and experimentally in references 14 to 21. Flight data have also provided some knowledge of the response of buildings to an imposed sonic-boom overpressure (refs. 22 and 23), and the psychological reaction of personnel exposed to various overpressure levels has also been explored (refs. 23 and 24).

The purpose of this report is to outline theoretical estimation methods, including a numerical evaluation of sonic-boom theory for use on high-speed

electronic computing machines, and to illustrate the correlation of this theory with wind-tunnel and flight measurements. Primary emphasis is placed on tunnel data from various sources which have been selected and presented to illustrate, in summary form, the more significant findings. Improved data-reduction methods and more precise theoretical estimation procedures than were employed in previous work have been used in the present correlations of theory with wind-tunnel data. Data-reduction procedures used herein provide for an adjustment to compensate for model vibration and other experimental limitations. Throughout this report, theoretical estimates are based on area distributions obtained from supersonic-area-rule cutting planes. The dependence of sonic-boom overpressure on configuration geometry is examined in some detail, and design methods of minimizing the problem are explored. Inasmuch as the discussions in this report are based, in large part, on wind-tunnel test results, they are necessarily restricted to the steady-state case of constant Mach number and altitude.

SYMBOLS

A	cross-sectional area of airplane or model determined by supersonic-area-rule cutting planes having an angle μ with respect to horizontal
$A(t)$	nondimensionalized cross-sectional area A/l^2 at nondimensionalized station $t = x/l$
A_b	cross-sectional area at base of airplane or model
A_e	nondimensionalized effective cross-sectional area due to a combination of volume and lift effects, $A(t) + B(t)$
$A_{e,n}, A_{e,r}$	nondimensionalized effective cross-sectional area A_e at nondimensionalized station $t = n\,\Delta t$ and $t = r\,\Delta t$, respectively
B	equivalent cross-sectional area due to lift, $\frac{\beta}{2q}\int_0^x F_L\,dx$
$B(t)$	nondimensionalized equivalent cross-sectional area due to lift B/l^2 at nondimensionalized station $t = x/l$
C_L	lift coefficient
F_L	lifting force per unit length along longitudinal axis of airplane or model
$F(\tau)$	effective area distribution function, $\frac{1}{2\pi}\int_0^\tau \frac{A_e''}{\sqrt{\tau - t}}\,dt$

h	airplane flight altitude or perpendicular distance from model to measuring probe
K_r	reflection factor
l	airplane or model reference length
M	Mach number
n,r	integers
p	reference pressure for a uniform atmosphere (free-stream static pressure for wind-tunnel tests)
$\overline{p}$	mean reference pressure for a nonuniform atmosphere determined by method given in reference 18
p_a	atmospheric pressure at airplane altitude
p_g	atmospheric pressure at ground level
Δp	incremental pressure due to flow field of airplane or model
Δp_{max}	maximum value of Δp (at bow shock)
q	dynamic pressure
S	wing planform area
t	nondimensionalized distance measured along longitudinal axis from airplane nose or model nose, x/l
Δt	incremental nondimensionalized distance along longitudinal axis of airplane or model
W	airplane weight
x	distance measured along longitudinal axis from airplane nose or model nose
ΔX	distance from point on pressure signature to point where pressure-signature curve crosses zero-pressure reference axis
δX	change in position of bow shock due to vibration
α	angle of attack

$$\beta = \sqrt{M^2 - 1}$$

γ ratio of specific heats (1.4 for air)

μ Mach angle, $\sin^{-1}\frac{1}{M}$

τ dummy variable of integration measured in same direction and using same units as t

τ_0 value of τ giving largest positive value of integral $\int_0^{\tau} F(\tau)\, d\tau$

A prime is used to indicate a first derivative and a double prime is used to indicate a second derivative with respect to distance.

NATURE OF THE PHENOMENON

The nature of the airplane shock field responsible for the sonic-boom phenomenon is illustrated in the schematic diagram of figure 1. At supersonic speeds the airplane-generated flow field is concentrated within a bow shock and a tail shock fanning out from the airplane. When these shock waves reach the ground, they are reflected upward. The shock waves traveling with the airplane and passing over the ground produce the noise sensed by the observer. Near the airplane the pressure signature is quite complex since it contains shock waves from the airplane nose, wing-fuselage juncture, engines, tail surfaces, and other airplane components. As the distance from the airplane increases, the separate shock waves merge and only a bow and a tail shock remain. The resultant N-shape wave signifies the attainment of the so-called far-field conditions. At ground level, the incident and reflected signatures are coincident and an amplification of the pressure rise occurs. On a hard level surface, a doubling

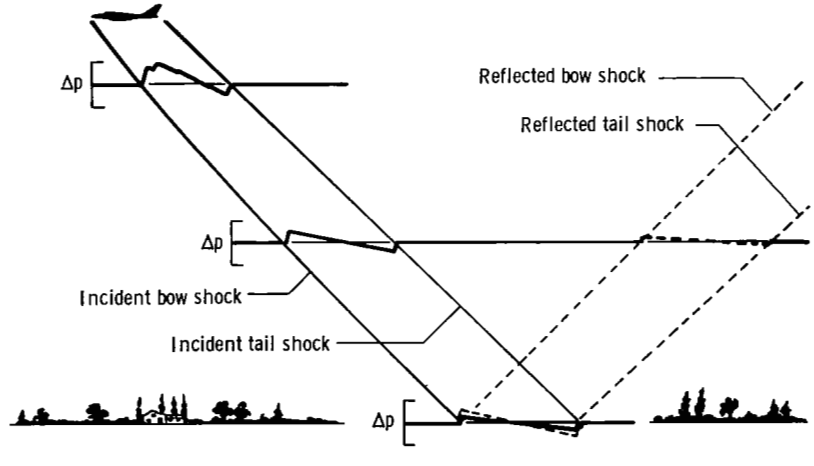

Figure 1.- Airplane shock field.

of the pressures takes place. For other surfaces, this reflection factor may be somewhat less than 2.0. In free air, in the absence of any reflecting surfaces, this reflection factor may be assumed to be 1.0.

THEORETICAL CONSIDERATIONS

The theoretical studies of references 1 to 3 have provided a means of estimating the bow-shock pressure rise. In the following equation obtained from reference 3, the bow-shock overpressure directly under the flight path of an airplane in level supersonic flight is related to the geometry of the airplane and the flight conditions:

$$\frac{\frac{\Delta p_{max}}{p}\left(\frac{h}{l}\right)^{3/4}}{K_r \beta^{1/4}} = \frac{1.19\gamma}{\sqrt{\gamma + 1}} \sqrt{\int_0^{\tau_0} F(\tau)\, d\tau} \qquad (1)$$

The function $F(\tau)$ in equation (1) depends on the longitudinal distribution of cross-sectional area and of lift and is defined as follows:

$$F(\tau) = \frac{1}{2\pi} \int_0^{\tau} \frac{A''(t)}{\sqrt{\tau - t}}\, dt + \frac{1}{2\pi} \int_0^{\tau} \frac{B''(t)}{\sqrt{\tau - t}}\, dt \qquad (2)$$

where $A''(t)$ represents the second derivative of a distribution along the longitudinal axis of a nondimensionalized airplane cross-sectional area determined by supersonic-area-rule cutting planes (as shown in fig. 2), and $B''(t)$ represents the second derivative of a distribution of nondimensionalized equivalent area due to lift evaluated through an integration of the lifting force per unit length along the airplane longitudinal axis. Typical airplane distributions are shown in figure 2. Since only the pressure field directly under the flight path of the airplane is being considered in this study, only one set of cutting planes having an angle μ with respect to the horizontal is used. Improved accuracy results when the area distributions include the increases in cross-sectional area due to boundary-layer thickness and engine-exhaust effects.

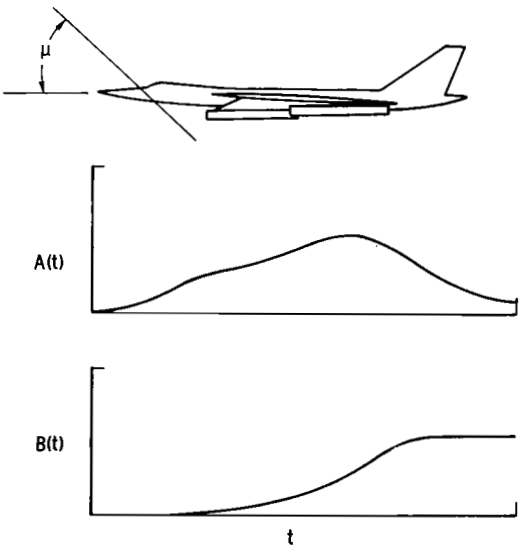

Figure 2.- Typical distributions used in sonic-boom theory.

Inasmuch as the sum of the derivatives is equal to the derivative of the sum, equation (2) may be written as

$$F(\tau) = \frac{1}{2\pi} \int_0^{\tau} \frac{A_e''}{\sqrt{\tau - t}} \, dt \tag{3}$$

where A_e'' is the second derivative of an effective cross-sectional area combining actual cross-sectional area with the equivalent cross-sectional area due to lift. This effective cross-sectional area is

$$A_e = A(t) + B(t) \tag{4}$$

The concept of effective cross-sectional area has been used in simplifying the numerical method of evaluating sonic-boom characteristics (presented in appendix A) and has been useful in defining the lower bound of sonic-boom overpressures discussed in the section entitled "Sonic-Boom Minimization Concepts."

The length of the positive portion of the pressure signature can be expressed by the following equation obtained from reference 3:

$$\frac{\Delta X}{l}\left(\frac{h}{l}\right)^{-1/4} = 1.19 \frac{\gamma + 1}{\sqrt{\gamma + 1}} \frac{M^2}{\beta^{3/4}} \sqrt{\int_0^{\tau_0} F(\tau) \, d\tau} \tag{5}$$

The slope of the linear portion of the signature may thus be written in the following form, which shows its independence of airplane geometry:

$$\frac{\Delta p}{\Delta X} = K_r \frac{p}{h} \frac{\beta}{M^2} \frac{\gamma}{\gamma + 1} \tag{6}$$

The theoretical estimation methods just described have been employed throughout the present report. In some of the earlier literature dealing with tunnel measurements (refs. 4, 5, and 7), these methods were not strictly applied. For example, in certain instances a parabolic-body area distribution was substituted for the actual distribution and in other instances a distribution of normal cross-sectional areas was used instead of that derived from supersonic-area-rule cutting planes.

MODELS, APPARATUS, AND TESTS

The experimental models and apparatus used in wind-tunnel investigations of the sonic-boom phenomenon are unique in several respects. The small size of

the models required for an approach to far-field conditions of the flow field is perhaps the most unusual feature. For tests conducted in the Langley 4- by 4-foot supersonic pressure tunnel, model lengths ranging from 1/2 to 2 inches are required. These small-scale models must be built to extremely small tolerances and must incorporate all the major airplane components. A very sensitive pressure-measuring system is also a necessity, since changes in pressure as small as 0.02 pound per square foot must be detected in the model flow field. An added complication in the design of pressure instrumentation results from the relatively large deviations of the reference or free-stream static pressures from the nominal value due to time lag in the tunnel control systems. This reference pressure may vary as much as 4 pounds per square foot from the nominal value in a period of several minutes. Since steady-state tunnel-flow nonuniformities dictate that the measuring probes or orifices be fixed with respect to the tunnel in order to avoid extraneous pressure variations, a means of varying the model position during the test must be provided. Because of the vibration of the models and apparatus, as well as the presence of a boundary layer and the lack of attainment of true far-field conditions, the sharp pressure peaks predicted by theory and displayed in signatures measured in flight are not obtained. Experimental apparatus and techniques designed to overcome or compensate for these difficulties are discussed in the remainder of this section and in appendix B.

Two tunnel-apparatus arrangements found to yield satisfactory results in sonic-boom tunnel investigations at the Langley Research Center are shown in figure 3. In one system, the measurements are made at orifices in a reflection plate or boundary-layer bypass plate alined with the tunnel free stream; in the other system, the measurements are made by using static-pressure probes. Both systems employ a remote-control sting support for longitudinal positioning of the model during the investigations. The apparatus shown in figure 3(b) has been used for the more recent tests because it minimizes the boundary-layer effect on the measured pressure signatures.

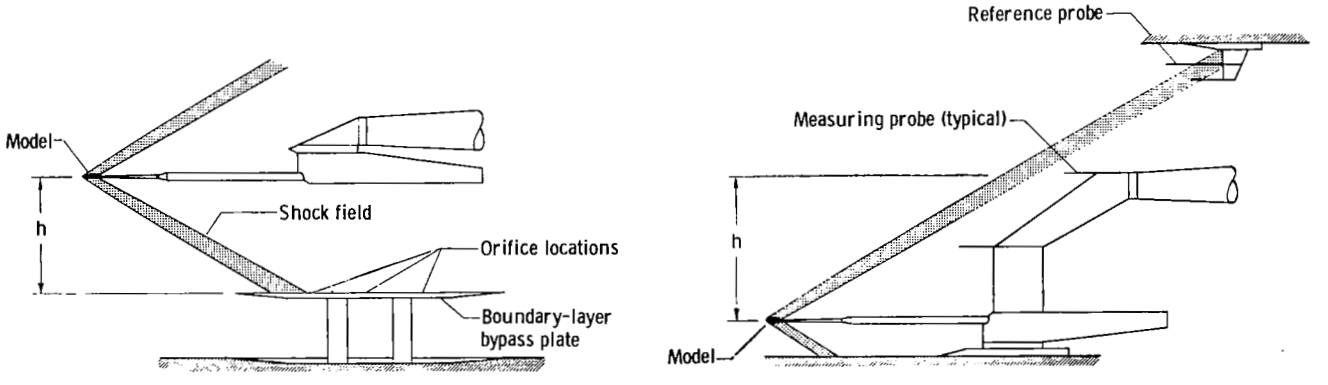

(a) Plate measurements.

(b) Probe measurements.

Figure 3. - Sketches of typical tunnel apparatus.

The schematic diagram of the pressure instrumentation shown in figure 4 is applicable for either of the arrangements shown in figure 3. Pressure gages having full-scale ranges as low as ±0.05 pound per square inch have been employed. The gage measures a pressure difference between the measuring probes or orifices and the reference probes or orifices. In order to avoid damage to the sensitive gage during tunnel startup and shutdown, a safety bypass valve has been provided. In the design of the instrumentation, deviations of the tunnel reference pressure from the nominal value have to be considered. Since it is only a pressure difference that is of concern, negligible errors result if changes in the measured reference pressure are immediately reflected in changes in the measured flow-field pressure. In effect, this situation can be brought about by equalizing the time lag in the instrumentation system on the two sides of the gage. Lengths and diameters of tubing are carefully balanced, and any remaining differences in time lag are compensated through use of a small variable-volume device (a bellows). Balancing of the system may be performed during tunnel evacuation or pressurization prior to a tunnel run.

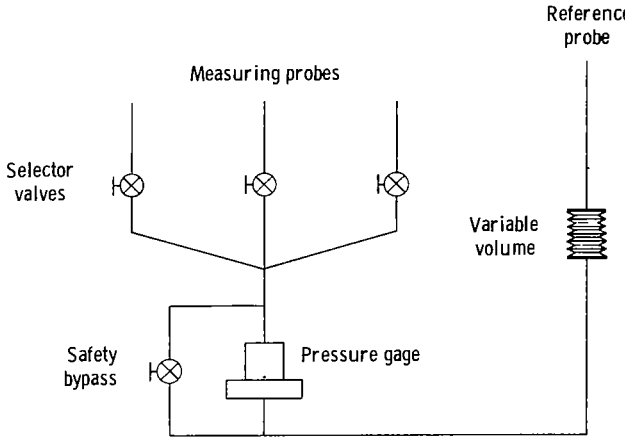

Figure 4. - Schematic diagram of pressure instrumentation.

A typical measured wind-tunnel pressure signature is shown in figure 5. According to theory, supported by flight-test evidence, the pressure signature on the ground from an airplane in supersonic flight will have (except at very low altitudes) a sharp-peaked N-shape similar to that shown by the dashed line. Departures of the measured wind-tunnel pressure signature from a true sharp-peaked N-shape wave are caused by the presence of near-field effects (double peak) and effects of vibration and probe boundary layer (rounded peaks). In this report the tunnel data have been adjusted to compensate for these limitations simply by extending the linear portion of the measured curve and forming a right triangle whose area is equal to the area under the measured wave. This adjustment, however, must be applied with caution, since it has not been shown to be valid where near-field effects predominate and a reasonable approach to a far-field signature is not evidenced. The maximum value of the measured wind-tunnel bow-shock pressure rise Δp_{max}, as used throughout this study, has been obtained from the adjusted signature. The adjustment (discussed in appendix B) was not applied to the data of references 4 and 5; however, a somewhat similar adjustment procedure which differed in details of application was used in references 6 and 7.

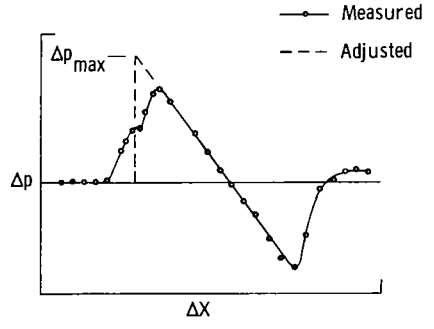

Figure 5. - Typical measured pressure signature.

MEASUREMENTS OF THICKNESS-INDUCED PRESSURES

Wind-tunnel measurements of the flow field surrounding several geometrically simple bodies (ref. 4) have allowed a study of thickness-induced sonic-boom characteristics. Representative data from that investigation, but now incorporating the adjustment discussed in appendix B, are presented in figures 6 to 8.

Bow-shock pressure rise obtained from adjusted pressure signatures for a nonlifting parabolic body of revolution (fineness ratio 5) is shown in figure 6 and is compared with theory. The theoretical curve presented differs to a small extent from that used in reference 4, since in the study presented herein the area distribution was determined by cutting planes inclined at the Mach angle rather than by planes normal to the body axis. The adjusted data display a remarkable agreement with the theoretical results both in magnitude and rate of decay with the distance from the model to the measuring probe, even for distances as close as 1 body length. Data for the parabolic body of revolution of figure 6 are shown in figure 7, in which a pressure parameter derived from theory (the left-hand side of eq. (1)) is employed. A constant value of the pressure parameter indicates a decay of overpressure with distance in accordance with the three-quarter-power rule of theory. The reflection factor for the boundary-layer bypass plate used in these tests was assumed to be 2.0.

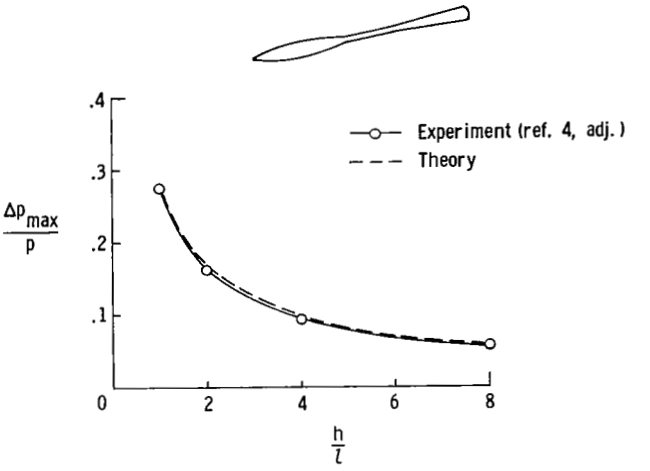

Figure 6. - Bow-shock pressure rise for a parabolic body of revolution as a function of distance. $M = 2.0$; $\alpha = 0^{o}$.

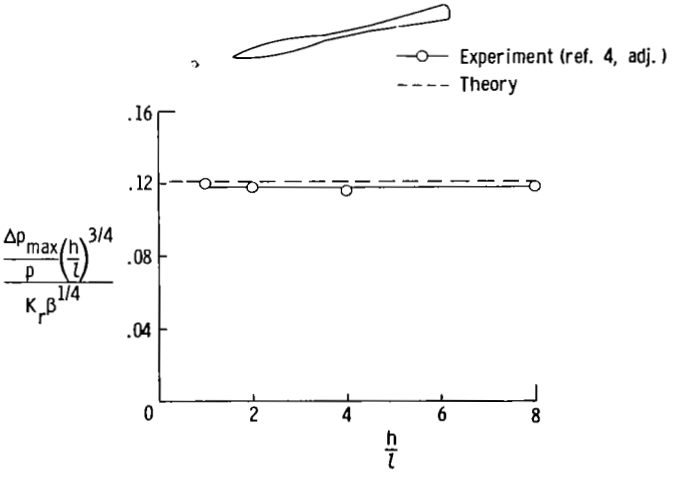

Figure 7. - Bow-shock pressure-rise parameter for the parabolic body of figure 6.

In figure 8, data are shown for a nonlifting body without axial symmetry. Although the overpressure measurements below the model and to the side are substantially different at a distance of 1 body length, they become more nearly equal at 8 body lengths - a result which indicates an approach to axial symmetry of the flow field. Theoretical estimates of pressures to the side of the model

are identical to those below the model rolled 90° when the supersonic-area-rule cutting planes remain at an angle μ with respect to the horizontal. Area distributions used in the theory are shown in the inset sketches. Although the shapes of the curves are different for the two model orientations, the maximum areas are identical and the theoretical pressure rise below the model is only slightly greater than that to the side. Since these differences are extremely small, the theoretical results presented in this figure are represented by a single line.

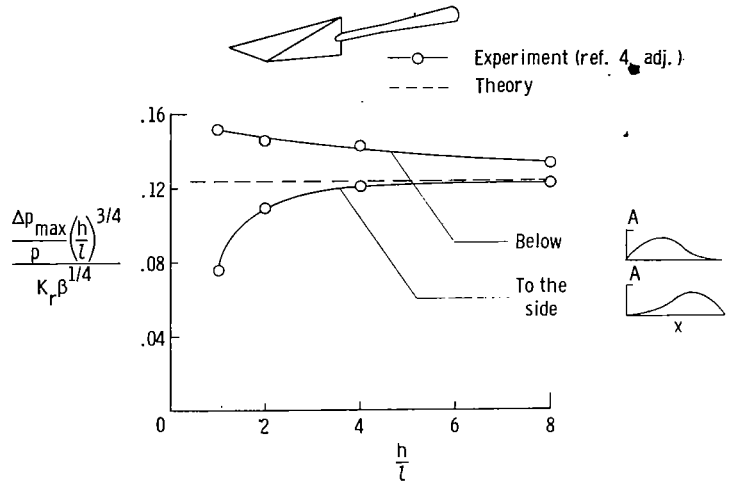

Figure 8. - Bow-shock pressure-rise parameter for a nonaxial symmetric body at zero lift. M = 2.0.

Data for a nonlifting body that departs radically from axial symmetry are shown in figure 9. (The model is actually a rectangular wing of aspect ratio 0.5 with a 12.5-percent-thick parabolic-arc section.) An examination of these data shows that even at 8 body lengths there are large differences in the measured pressures below and to the side of the model and that there appears to be little tendency toward a further approach to axial symmetry of the flow field. This result is in reasonable agreement with the theory, which also shows a large difference between overpressures below and to the side of the model. These differences are directly related to the area distributions formed by supersonic-area-rule cutting planes and shown on the right-hand side of the figure. The reduced overpressures to the side of the model are caused primarily by the increased length and reduced maximum cross-sectional area of the corresponding area distribution. These and other experimental investigations, both tunnel and flight tests, support the validity of the supersonic-area-rule equivalent-body concept in treating thickness-induced far-field pressures.

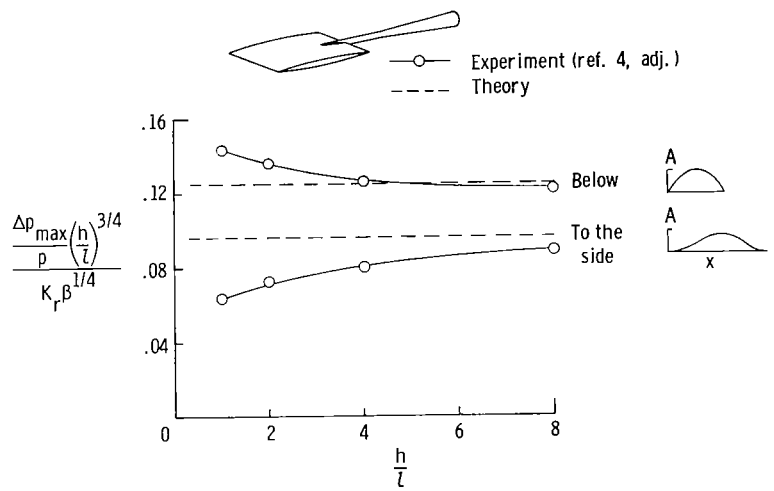

Figure 9. - Bow-shock pressure-rise parameter for a rectangular wing at zero lift. M = 2.0.

MEASUREMENTS OF LIFT-INDUCED PRESSURES

The influence of lift on sonic-boom overpressures may be studied by using the data for delta-wing configurations shown in figures 10 and 11. The measurements of lift-induced pressures shown are taken from the investigation of reference 5 but they have now been subjected to the adjustment previously mentioned.

Bow-shock pressure rise below a 60° delta wing at angles of attack of 0°, 5°, and 10° and at $M = 2.0$ is shown in figure 10. Large differences in overpressure level due to angle of attack (or lift) may be observed in both the experimental and theoretical data. These differences may be attributed to differences in the area distributions shown on the right-hand side of the figure. The area distributions now include equivalent cross-sectional area due to lift.

In figure 11, overpressure characteristics for a series of related wing-body configurations are presented in a parametric form derived from theoretical relationships. Since the wing-body configurations were designed to have the same distribution of cross-sectional area and since the delta wings have the same equivalent cross-sectional area due to lift at a given value of the parameter $\frac{\beta}{2} C_L \frac{S}{l^2}$, a single curve should serve as the theoretical estimate for the four configurations. However, because the cross-sectional area due to the displacement effect of the assumed laminar boundary layer varies depending upon the model wetted area, the theory is presented as a shaded band. Except in the immediate vicinity of $\frac{\beta}{2} C_L \frac{S}{l^2} = 0$, experimental results are in good agreement with theory, both in magnitude and trend. The experimental data shown in this figure are for a distance of 32 body lengths; however, the data should apply for greater distances since far-field conditions have nearly been achieved, as indicated in figure 10 by the small or nonexistent slope of the pressure parameter with distance at 32 body lengths.

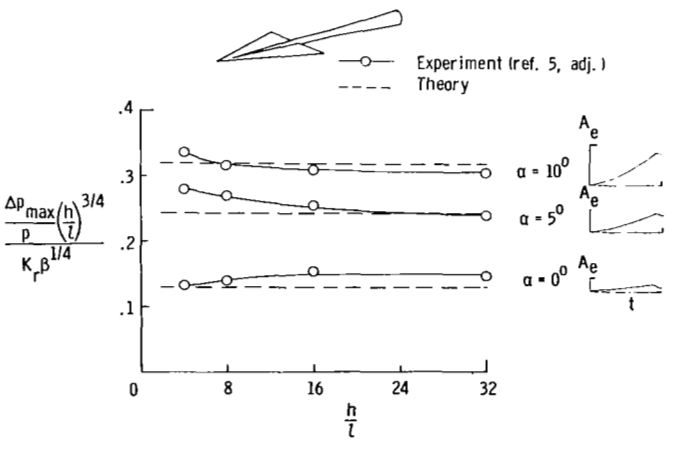

Figure 10. - Bow-shock pressure-rise parameter for a lifting delta-wing configuration. $M = 2.0$.

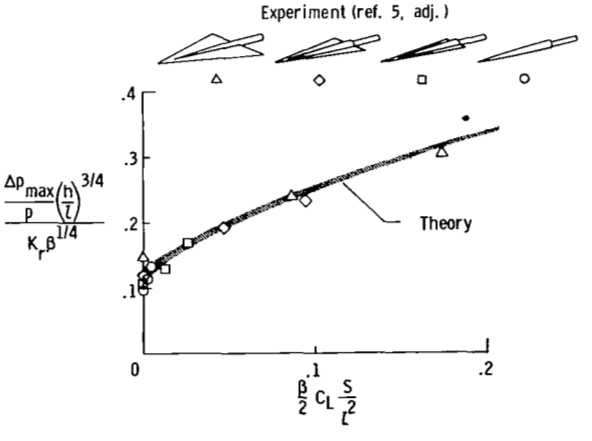

Figure 11. - Bow-shock pressure-rise parameter for a series of wing-body configurations as a function of lift parameter. $M = 2.0$; $h/l = 32$.

CORRELATION OF WIND-TUNNEL AND FLIGHT DATA

A comparison of tunnel-measured bow-shock pressure rise at $M = 2.0$ and $h/l = 50$ for a complete supersonic bomber airplane configuration (ref. 6) with a theoretical estimate of the pressure rise determined in the manner described in appendix A is shown in figure 12. The area distribution used in the theoretical estimate included the cross-sectional area due to the displacement thickness of a laminar boundary layer. The figure shows close agreement between wind-tunnel measurements and theoretical overpressure values.

Flight-test results for the supersonic bomber airplane are reported in reference 12. These tests have produced the most extensive and most self-consistent data yet recorded for ground measurements of the sonic boom created by an airplane. The instrumentation employed is noteworthy in that it faithfully reproduced the entire pressure signature and not just the peaks as in previous tests (for example, refs. 9 to 11). The data are of particular interest since the altitude range extends to 75,000 feet where lift effects are important. Correlation of these flight data with theoretical estimates in a manner similar to that used for the correlation of the tunnel data is possible for this same airplane. However, for use in equation (1), it is first necessary to define a reference pressure which accounts for the variation of atmospheric pressure and temperature between the airplane and the ground. In most previous work, a crude approximation, the geometric mean of the atmospheric pressure at altitude and that on the ground $\left(\sqrt{p_a p_g}\right)$, has been used. A thorough study of the effects of the atmosphere given in reference 18 provides an evaluation of shock strength as the shock propagates through the layers of an assumed stratified atmosphere. From such information for a standard atmosphere supplied by the authors of reference 18, a mean or effective reference pressure $\bar{p}$ has been evaluated and the ratio $\bar{p}/\sqrt{p_a p_g}$ is presented in figure 13. Note that at the altitudes normally associated with supersonic flight, $\bar{p}$ is substantially greater than $\sqrt{p_a p_g}$.

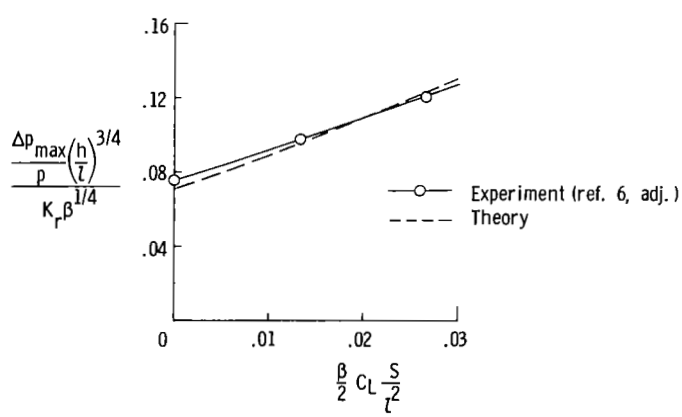

Figure 12. - Bow-shock pressure-rise parameter for a wind-tunnel model of a supersonic bomber airplane. $M = 2.0$; $h/l = 50$.

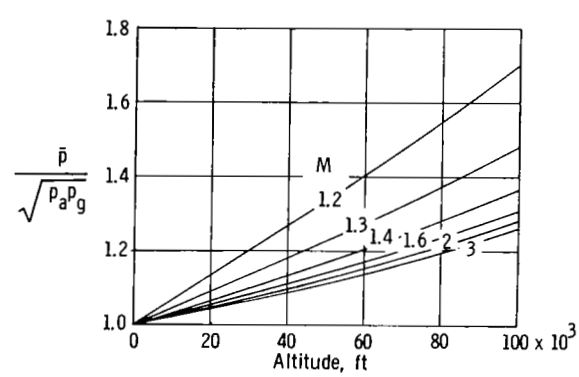

Figure 13. - Ratio of mean reference pressure (determined by method of ref. 18) to geometric mean.

With the use of the mean reference pressure $\bar{p}$, the flight data for the supersonic bomber airplane (ref. 12) may be reduced to the parametric form shown in figure 14. Each data point represents the average pressure rise recorded by several microphones in use during a given overpass. These microphones were spaced along the airplane ground track over a distance of about 4 miles. A reflection factor of 2.0 was used in evaluating the pressure-rise parameter since measurements during the test indicated that the dry lakebed over which the flights were conducted acted as a nearly perfect reflection plane. The flight data show overpressures slightly higher than the theoretical estimates in which an increase in cross-sectional area due to a turbulent boundary layer has been included. On the average, the measured results fall about 5 percent higher than the theoretical estimates; however, the variation with lift parameter is in close agreement with the theory. The tunnel data of figure 12 and the flight data of figure 14 provide strong evidence that lift effects are well predicted with present-day theoretical estimation methods. In addition, these data tend to indicate that atmospheric effects may be better accounted for by using the methods of reference 18 than by using previous methods.

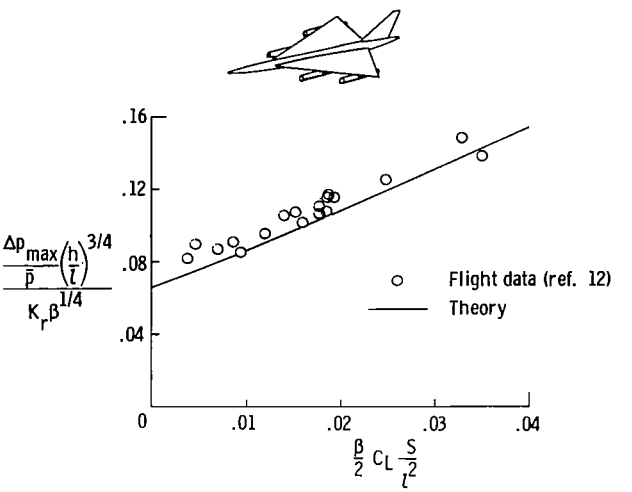

Figure 14. - Flight measurements of bow-shock pressure-rise parameter for a supersonic bomber airplane. M = 1.5 to 2.0.

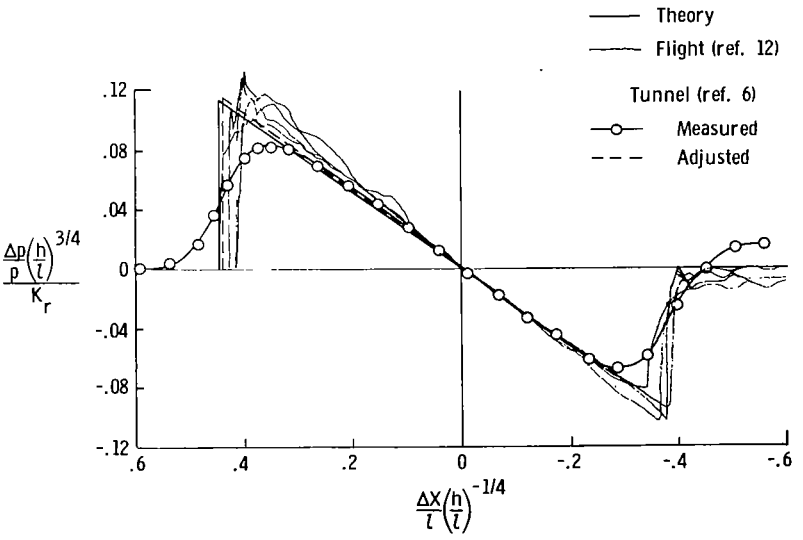

Figure 15. - Comparison of flight and tunnel measurements of pressure signature of a supersonic bomber airplane. M = 2.0; $\frac{\beta}{2} C_L \frac{S}{l^2} = 0.0135$.

A direct comparison of pressure signatures measured in the flight test with a signature measured in the tunnel test is shown in figure 15. This comparison has been made possible through a correspondence in Mach number and lift coefficient for a flight data point and a tunnel data point. Representative signatures from four of the microphones in use during the overpass (including the maximum and minimum pressure peaks) are compared with the tunnel measurement and

with theory. The dashed line, which represents an adjusted tunnel signature as defined in appendix B, displays a reasonable agreement with the flight signatures.

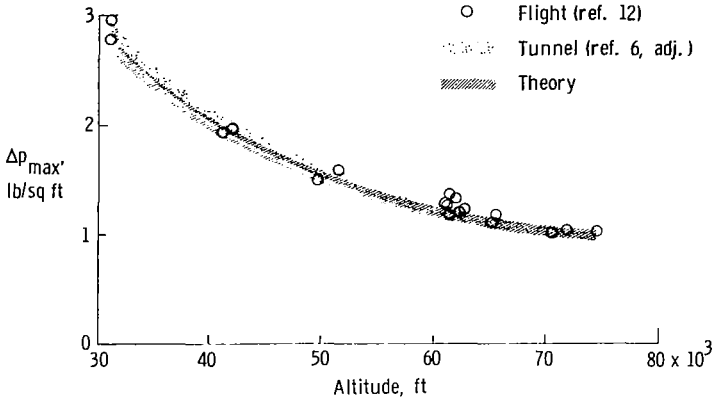

Figure 16. - Flight measurements of ground overpressures for a supersonic bomber airplane. M = 1.5 to 2.0.

A more familiar form for the presentation of flight sonic-boom data than the parametric form used in figure 14 is given in figure 16. Average values of the maximum ground-measured overpressures are plotted as a function of altitude. The estimates, based on theory and on extrapolated tunnel data, are shown as a band in order to account for variations in flight Mach number and airplane weight at a given altitude. The range of Mach numbers from 1.5 to 2.0 and the range of airplane weights from 62,000 to 92,000 pounds account for a much narrower band than is shown by the scatter of the data. Nevertheless, the agreement of the flight data with the estimates is generally good and indicates, to some extent, the degree of confidence which may be placed in further estimates of nominal ground overpressure using these methods.

SONIC-BOOM MINIMIZATION CONCEPTS

The theory of references 1 to 3 has made possible the definition of a lower bound of sonic-boom overpressure, which has been discussed in references 25 and 26. As shown previously, sonic-boom strength depends on an effective area distribution in which both volume and lift components are combined. An example of an effective-area-distribution curve is shown in figure 17. Note that the value of A_e at the base of the airplane is fixed by the airplane base area (including boundary-layer and engine-exhaust areas) and by the flight conditions of Mach number and lift coefficient. Although the sonic-boom strength parameter has been found to depend primarily on the value of the effective cross-sectional area at the base, it also depends on the shape of the complete A_e curve. In reference 25 the shape of the area-distribution curve yielding a minimum sonic boom was shown to be given by a function in which the area is proportional to the square root of the distance from the nose except in the immediate vicinity of the airplane nose. Such a curve is shown by the dashed line of figure 17. As shown in reference 26, a lower bound of attainable sonic-boom overpressure that depends only

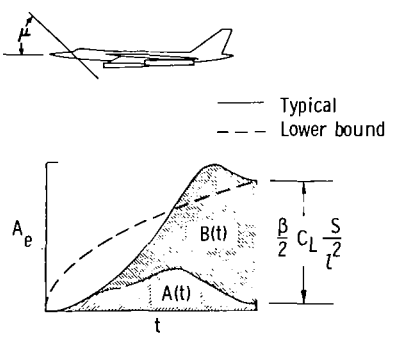

Figure 17. - Lower-bound effective-area distribution.

on the airplane length, weight, base area, and flight conditions can be written in simplified form as

$$\frac{\frac{\Delta p_{max}}{p}\left(\frac{h}{l}\right)^{3/4}}{K_r \beta^{1/4}} = 0.54\sqrt{\frac{\beta}{2} C_L \frac{S}{l^2} + \frac{A_b}{l^2}} \tag{7}$$

Although this form of the equation follows that used in reference 26, the shape of the optimum-area curve and the resultant shape factor of 0.54 were obtained with the use of reference 25. The lower-bound expression neglects any minimum-volume restrictions and thus is inapplicable near zero lift coefficient, as explained in reference 26. This omission has not proved to be serious in the studies made to date. When volume restrictions become necessary, they may be included, as was done in reference 26. In the limiting case when A_b is zero, the lower-bound expression may be written as

$$\frac{\frac{\Delta p_{max}}{p}\left(\frac{h}{l}\right)^{3/4}}{K_r \beta^{1/4}} = 0.54\sqrt{\frac{\beta}{2} C_L \frac{S}{l^2}} = 0.54\sqrt{\frac{\beta}{2} \frac{W}{q l^2}} \tag{8}$$

The lower-bound concept not only sets limits on attainable overpressures but also suggests design methods of approaching these limiting values. Theoretically, for a selected flight condition (a design point), it should be possible to design a configuration to approach the sonic-boom minimization requirements. Some experimental data (ref. 7) believed to be applicable in connection with these concepts are shown in figure 18. Measured and theoretical overpressures in parametric form have been plotted against the lift parameter for two wing-body models. The model with the wing in the rearward location theoretically approaches the lower bound even though it was not designed strictly in accordance with the concepts previously discussed. Effective-area-distribution curves for an assumed design point $\left(\frac{\beta}{2} C_L \frac{S}{l^2} = 0.0086\right)$ are shown on the right-hand side of the figure. These curves illustrate graphically that the area distribution of the rear-wing model more closely

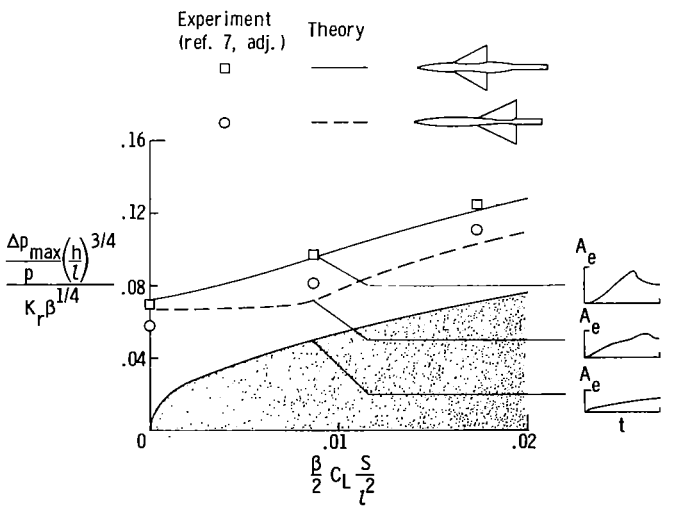

Figure 18. - Comparison of sonic-boom characteristics of configurations approaching, to different degrees, the requirements for lower bound. M = 2.0; h/l = 50.

approaches that of the lower bound. The experimental results confirm the trends predicted by theory. Reference 27 provides a study of the effects of the necessary compromises with airplane drag on the attainment of sonic-boom lower bound.

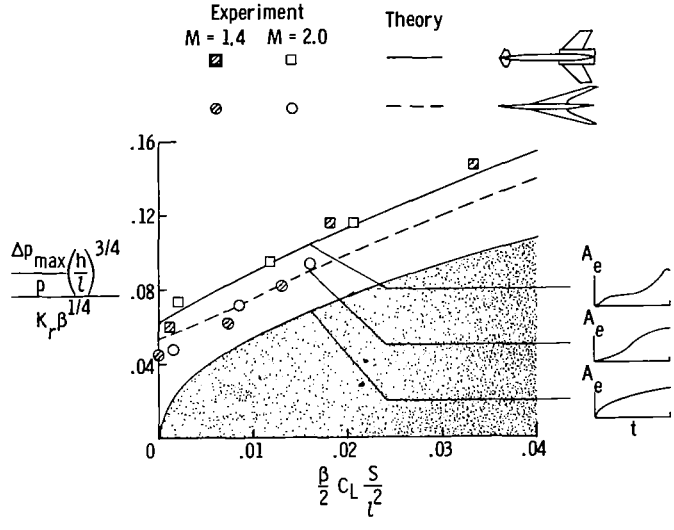

Figure 19. - Comparison of sonic-boom characteristics of two supersonic transport configurations. M = 1.4 and 2.0; $h/\ell = 50$.

In order to provide an illustration of configuration effects, a comparison of the sonic-boom characteristics of two transport configuration models is shown in figure 19. Both theoretical and experimental wind-tunnel data are shown and are compared with a lower-bound curve for which the base area A_b is assumed to be zero. Inasmuch as theoretical differences in the sonic-boom characteristics at the two Mach numbers are small, only a single curve is shown for each configuration. Cross-sectional areas used in the theory include the area within the estimated displacement thickness of a laminar boundary layer. The lower overpressures for the arrow-wing design may be attributed to the reduced base area and to the smoother area- and lift-distribution curves. Examples of effective-area-distribution curves for an arbitrarily selected value of the lift parameter are also shown in the figure. These data illustrate the significant effect of configuration geometry on sonic-boom strength.

CONCLUDING REMARKS

A review and analysis of wind-tunnel and flight sonic-boom data incorporating recent developments in wind-tunnel data-reduction methods has reaffirmed the conclusion that both volume and lift effects contribute to bow-shock overpressures. The study has also shown that existing theory provides reasonably accurate estimates of nominal ground-track boom overpressures for steady flight in a standard or near-standard atmosphere. It has been indicated, however, that design considerations based on developments of the theory will be only partly effective in minimizing the sonic-boom problem.

Langley Research Center,
National Aeronautics and Space Administration,
Langley Station, Hampton, Va., August 7, 1964.

APPENDIX A

A NUMERICAL EVALUATION OF SONIC-BOOM THEORY FOR USE ON HIGH-SPEED ELECTRONIC COMPUTING MACHINES

Theoretical estimates based on the work of references 1 to 3 and used in this report for correlation with the experimental data have been evaluated by using a numerical procedure. Because of the nature of the curve-fitting technique employed, the area distributions are made to be smooth (that is, having no discontinuity in the first derivative). Thus, rather than by employing more rigorous solution suggested in reference 2, discontinuities in the first derivative are accounted for by assuming the changes to occur over finite distances.

As discussed previously, configuration sonic-boom characteristics are directly dependent on an effective-area-distribution curve A_e formed by a direct addition of actual area and equivalent area due to lift. As shown in figure A1, the A_e curve may be approximated by a series of parabolic arcs having a first derivative composed of continuous straight-line segments and a second derivative composed of a step or pulse function. The integral involved in the $F(\tau)$ function can be evaluated quite easily when A_e'' is a constant; and by superposition, a complete $F(\tau)$ curve may be built up corresponding to the A_e'' pulse distribution. An integration of the $F(\tau)$ function to the point τ_0 (cross-hatched area in fig. A1) is then used in evaluating the right-hand side of equation (1). The degree of approximation of the A_e curve can be improved by increasing the number of pulses used.

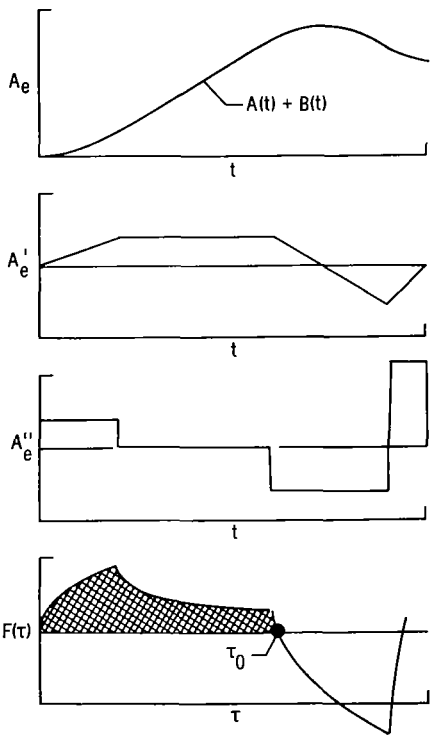

Figure A1. - Numerical method of determining sonic-boom characteristics.

The effective nondimensionalized cross-sectional area may be expressed as

$$A_e = \frac{A}{l^2} + \frac{\beta}{2} C_L \frac{S}{l^2}\left[\frac{\int_0^x F_L \, dx}{\int_0^l F_L \, dx}\right]$$

or

$$A_e = A(t) + \frac{\beta}{2} C_L \frac{S}{l^2}\left[\frac{B(t)}{B(1)}\right] \tag{A1}$$

If it is assumed that local lifting pressures are directly proportional to the total lift coefficient, the quantity in brackets in equation (A1) is a constant for any airplane station. The inputs to the program are thus tabulations of $A(t)$ and $B(t)/B(1)$ as functions of equally spaced nondimensionalized airplane stations. Equation (A1) then allows an evaluation and tabulation of the effective area distribution A_e for selected values of the lift parameter $\frac{\beta}{2} C_L \frac{S}{l^2}$.

A series of parabolas, fitted to these points so that the resultant curve has no discontinuities in slope, may be expressed as follows:

$$\left.\begin{aligned}
A_{e,1} &= \frac{A_{e,1}}{(\Delta t)^2} t^2 && (0 < t < \Delta t)\\
A_{e,2} &= A_{e,1} + A'_{e,1}(t - \Delta t) + \frac{\left(A_{e,2} - A_{e,1}\right) - \left(A'_{e,1}\right)\Delta t}{(\Delta t)^2}(t - \Delta t)^2 && (\Delta t < t < 2\Delta t)\\
A_{e,3} &= A_{e,2} + A'_{e,2}(t - 2\Delta t) + \frac{\left(A_{e,3} - A_{e,2}\right) - \left(A'_{e,2}\right)\Delta t}{(\Delta t)^2}(t - 2\Delta t)^2 && (2\Delta t < t < 3\Delta t)\\
A_{e,n} &= A_{e,n-1} + A'_{e,n-1}\left[t - (n-1)\Delta t\right] + \frac{\left(A_{e,n} - A_{e,n-1}\right) - \left(A'_{e,n-1}\right)\Delta t}{(\Delta t)^2}\left[t - (n-1)\Delta t\right]^2 && \left((n-1)\Delta t < t < n\Delta t\right)
\end{aligned}\right\} \tag{A2}$$

The second derivative is

$$\left.\begin{aligned}
A''_{e,1} &= \frac{2}{(\Delta t)^2} A_{e,1} && (0 < t < \Delta t)\\
A''_{e,2} &= \frac{2}{(\Delta t)^2}\left(A_{e,2} - A_{e,1}\right) - 2A''_{e,1} && (\Delta t < t < 2\Delta t)\\
A''_{e,3} &= \frac{2}{(\Delta t)^2}\left(A_{e,3} - A_{e,2}\right) - 2\left(A''_{e,1} + A''_{e,2}\right) && (2\Delta t < t < 3\Delta t)\\
A''_{e,n} &= \frac{2}{(\Delta t)^2}\left(A_{e,n} - A_{e,n-1}\right) - 2\sum_{r=1}^{r=n-1} A''_{e,r} && \left((n-1)\Delta t < t < n\Delta t\right)
\end{aligned}\right\} \tag{A3}$$

The $F(\tau)$ function then becomes

$$\left.\begin{aligned}
F(\tau) &= \frac{1}{\pi} A''_{e,1}\sqrt{\tau} && (0 < t < \Delta t)\\
F(\tau) &= \frac{1}{\pi}\left[A''_{e,1}\sqrt{\tau} + \left(A''_{e,2} - A''_{e,1}\right)\sqrt{\tau - \Delta t}\right] && (\Delta t < \tau < 2\Delta t)\\
F(\tau) &= \frac{1}{\pi}\left[A''_{e,1}\sqrt{\tau} + \left(A''_{e,2} - A''_{e,1}\right)\sqrt{\tau - \Delta t} + \left(A''_{e,3} - A''_{e,2}\right)\sqrt{\tau - 2\Delta t}\right] && (2\Delta t < \tau < 3\Delta t)\\
F(\tau) &= \frac{1}{\pi}\sum_{r=1}^{r=n}\left(A''_{e,r} - A''_{e,r-1}\right)\sqrt{\tau - (r-1)\Delta t} && ((n-1)\Delta t < \tau < n\Delta t)
\end{aligned}\right\} \quad (A4)$$

and the integral of the $F(\tau)$ function may be written as

$$\left.\begin{aligned}
\int_0^{\tau=\Delta t} F(\tau)d\tau &= \frac{2}{3\pi} A''_{e,1}(\Delta t)^{3/2}\\
\int_0^{\tau=2\Delta t} F(\tau)d\tau &= \frac{2}{3\pi}\left[A''_{e,1}(2\Delta t)^{3/2} + \left(A''_{e,2} - A''_{e,1}\right)(\Delta t)^{3/2}\right]\\
\int_0^{\tau=3\Delta t} F(\tau)d\tau &= \frac{2}{3\pi}\left[A''_{e,1}(3\Delta t)^{3/2} + \left(A''_{e,2} - A''_{e,1}\right)(2\Delta t)^{3/2} + \left(A''_{e,3} - A''_{e,2}\right)(\Delta t)^{3/2}\right]\\
\int_0^{\tau=n\Delta t} F(\tau)d\tau &= \frac{2}{3\pi}\sum_{r=1}^{r=n}\left(A''_{e,r} - A''_{e,r-1}\right)\left[(n - r + 1)\Delta t\right]^{3/2}
\end{aligned}\right\} \quad (A5)$$

The area-distribution curve-fitting technique employed produces solutions for the derivatives, the $F(\tau)$ function, and the integral of $F(\tau)$ that oscillate from point to point. From comparisons of numerical solutions with certain analytical solutions for simple bodies, these oscillations have been found to center on the analytical solutions. Improved accuracy results when the integral of $F(\tau)$ is averaged as follows:

$$\begin{aligned}
\int_0^{\tau=n\Delta t} F(\tau)d\tau = {} & \frac{1}{3\pi}\sum_{r=1}^{r=n}\left(A''_{e,r} - A''_{e,r-1}\right)\left[(n - r + 1)\Delta t\right]^{3/2}\\
& + \frac{1}{6\pi}\sum_{r=1}^{r=n-1}\left(A''_{e,r} - A''_{e,r-1}\right)\left[(n - r + 1)\Delta t\right]^{3/2}\\
& + \frac{1}{6\pi}\sum_{r=1}^{r=n+1}\left(A''_{e,r} - A''_{e,r-1}\right)\left[(n - r + 1)\Delta t\right]^{3/2}
\end{aligned} \quad (A6)$$

Finally, the overpressure is found by selecting the maximum value of equation (A6) and substituting it into the following equation:

$$\frac{\left(\frac{\Delta p}{p}\right)_{max}\left(\frac{h}{l}\right)^{3/4}}{K_r \beta^{1/4}} = \frac{1.19\gamma}{\sqrt{\gamma + 1}}\sqrt{\left[\int_0^{\tau=n\Delta t} F(\tau)d\tau\right]_{max}} \tag{A7}$$

Equations (A1) to (A7) can be readily adapted for use on high-speed electronic computing machines in a numerical evaluation of sonic-boom theory. The computational program may be summarized as follows. The inputs are tabulations of the nondimensionalized area $A(t)$ and the integrated lift distribution ratio $B(t)/B(1)$ as functions of equally spaced nondimensionalized airplane stations. Equation (A1) then allows the determination of a table of effective cross-sectional areas for preselected values of the lift parameter $\frac{\beta}{2} C_L \frac{S}{l^2}$. The second-derivative step function is then generated by using equation (A3). Tabulated values of A_e'' are used in evaluating equation (A6), the maximum value of this integral being selected and used in equation (A7) to evaluate the sonic-boom characteristics of the configuration. For airplane configurations employing camber, the loading distribution at zero lift may be taken into account by using a modified area distribution. In this case $\frac{A}{l^2}$ is replaced by $\frac{A}{l^2} + \frac{\beta}{2ql^2}\int_0^x F_L\, dx$ where F_L is the lifting force per unit length at zero lift.

APPENDIX B

ADJUSTMENTS OF WIND-TUNNEL MEASUREMENTS OF BOW-SHOCK STRENGTH TO COMPENSATE FOR EXPERIMENTAL LIMITATIONS

A number of experimental difficulties arise in attempting to measure within the confines of a wind tunnel the pressure signatures of the necessarily small models and in attempting to extend the results to apply to full-size airplanes at flight altitudes. The necessity of attaining or approaching far-field conditions, where the pressure signature assumes a characteristic N-shape, requires that tunnel models be extremely small. Even with models as small as those employed in the investigations of this report, an approach to far-field conditions is not achieved in all cases. It does not appear to be practical to reduce further the model size because of construction difficulties and because vibrations of models, probes, and support apparatus introduce changes in the shape of the pressure signature and in the magnitude of the pressure rise, which become progressively more pronounced as model size is decreased. The presence of a boundary layer on the measuring probe also introduces changes in the shape of the signature and in the magnitude of the pressure rise, which are dependent on model size. Another result of decreased model size is the increase in relative importance of the increment in effective cross-sectional area due to model boundary layer.

With a compromise model size, the experimental limitations in attaining a far-field N-shape pressure signature are always present to some degree and are occasionally large. Thus, a method of interpreting the results and compensating for these limitations becomes necessary. The following discussion explores these problems and describes the method used to adjust the wind-tunnel measurements of bow-shock strength.

The failure to achieve a classical N-shape wave in tunnel tests is due in part to the fact that in many cases the pressure signatures are in the transition region from near-field to far-field conditions, as shown by the data of figure B1. These measurements made at M = 2.0 for the canard transport configuration shown in figure 19 have been plotted in a parametric form suggested by theoretical considerations. According to the theory,

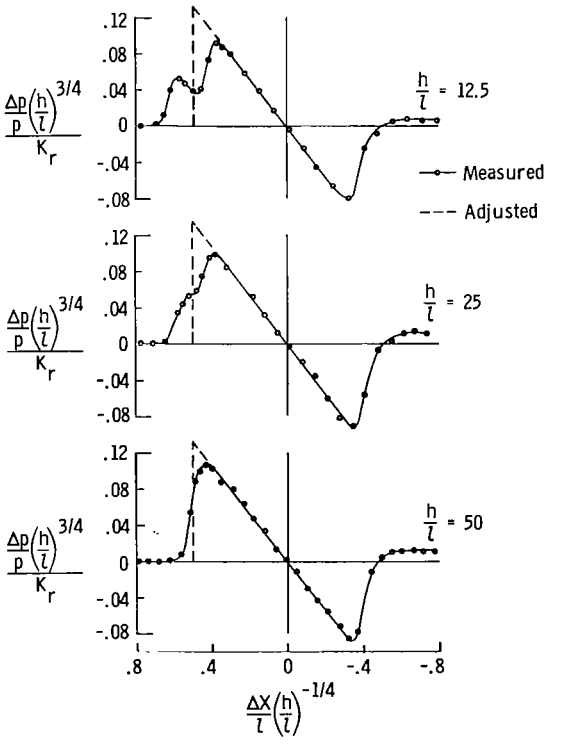

Figure B1. - Transition of pressure signature from near-field to far-field form.

when far-field conditions (an N-wave) have been achieved, signatures plotted in this form remain identical as distance is increased. The near-field shape of the pressure signature at $h/l = 12.5$ is evidenced by the presence of two distinct pulses in the region of the bow shock. These apparently are the separate shocks from the fuselage nose and from the wing-body juncture. At a distance of 50 body lengths, the pulses have merged and an N-shape wave is approached. It has been noted that even for quite complex signatures, a linear portion of the pressure signature develops and the slope closely agrees with that estimated by far-field theory. By accepting the premise that, during this transition (as far-field conditions are approached), the impulse area under the bow-shock portion of the signature attenuates with distance in a manner similar to that for a fully developed N-wave, an attempt may be made to define the pressure signature that would exist if far-field conditions were established. The adjusted signature may be determined as illustrated in figure B1 simply by extending the linear portion of the measured signature forward so that a right triangle is formed whose area is equal to the area under the measured curve. Because of inexactness in the assumptions, the adjustment cannot be rigorously correct; however, a practical test would appear to be met when adjusted signatures plotted in the form used in figure B1 remain constant as distance is increased. The remaining discrepancies between the measured signature at $h/l = 50$ and the sharp-peaked N-shape signature which would be expected in the far field are believed to be caused by vibrations of the model and support apparatus as well as by boundary-layer effects.

In order to study the influence of vibration, consider a completely steady model in uniform supersonic flow and an ideal pressure-sensing system with a probe at a distance large enough to enable a true far-field N-wave to be recorded, as represented by the long-dash line in figure B2. Suppose that the model (or the measuring probe) undergoes a constant-amplitude vibratory motion represented by the inset sketch. The N-wave will then occupy successive positions at equal time increments as indicated by the short-dash lines on the pressure signature plot. At a given longitudinal probe location, a highly damped measuring system such as the one used for these tests would register a time average of the pressures imposed on it. When a range of probe locations is considered, the measured pressure signatures with a constant-amplitude vibrating system take on the appearance of the solid-line curve. This curve does not resemble the actual wind-tunnel data, but it is not likely that tunnel vibration is confined to the single amplitude shown in figure B2. When a varying amplitude is considered, the resulting pressure signature assumes the characteristics of that shown in figure B3. The assumed amplitude-time relationship is shown in the inset sketch. The resulting signature now resembles those obtained from actual tunnel measurements.

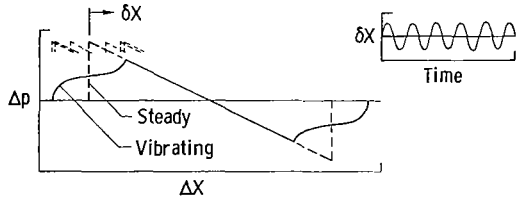

Figure B2. - Effect of constant-amplitude vibration.

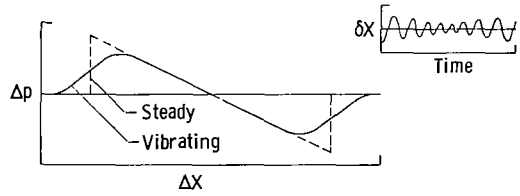

Figure B3. - Effect of varying-amplitude vibration.

In both figure B2 and figure B3, note that the areas under the curves are almost unchanged from the steady to the vibrating condition. Also note that the middle portion of the signature remains unaffected provided the amplitude of the vibration is less than the length of the signature. These observations may now be utilized in an attempt to adjust the measured data to provide an estimate of the pressure signature in the absence of vibration. This adjustment may be accomplished by extending the linear portion of the measured signature forward so that a right triangle is formed whose area is equal to the area under the measured curve. Since this procedure is identical to that previously discussed in the compensation for the presence of near-field pressure-signature characteristics, one adjustment will suffice for both deficiencies.

The foregoing discussion of vibration effects was considered to be independent of possible viscous effects. The probe boundary layer, however, is a significant factor in the sensing of static-pressure changes across shock waves. The imposition of shock-wave pressure gradients on boundary layers of pressure-sensing instruments generally produces flow distortions which can be sensed both upstream and downstream of shock locations. This condition effectively results in tendencies for instrument-sensed pressure changes across shock waves to be less abrupt than pressure discontinuities across the shock waves in the absence of instruments. Such effects of boundary layer, as well as effects of vibration, in spreading and rounding off shock-wave pressure signatures are approximately accounted for by the previously described technique for adjusting wind-tunnel pressure measurements. The applicability of the adjustment technique may be uncertain, however, if the pressure-sensing arrangements are different from those employed in these investigations.

REFERENCES

1. Whitham, G. B.: The Flow Pattern of a Supersonic Projectile. Communications on Pure and Appl. Math., vol. V, no. 3, Aug. 1952, pp. 301-348.

2. Whitham, G. B.: On the Propagation of Weak Shock Waves. J. Fluid Mech., vol. 1, pt. 3, Sept. 1956, pp. 290-318.

3. Walkden, F.: The Shock Pattern of a Wing-Body Combination, Far From the Flight Path. Aero. Quarterly, vol. IX, pt. 2, May 1958, pp. 164-194.

4. Carlson, Harry W.: An Investigation of Some Aspects of the Sonic Boom by Means of Wind-Tunnel Measurements of Pressures About Several Bodies at a Mach Number of 2.01. NASA TN D-161, 1959.

5. Carlson, Harry W.: An Investigation of the Influence of Lift on Sonic-Boom Intensity by Means of Wind-Tunnel Measurements of the Pressure Fields of Several Wing-Body Combinations at a Mach Number of 2.01. NASA TN D-881, 1961.

6. Carlson, Harry W.: Wind-Tunnel Measurements of the Sonic-Boom Characteristics of a Supersonic Bomber Model and a Correlation With Flight-Test Ground Measurements. NASA TM X-700, 1962.

7. Morris, Odell A.: A Wind-Tunnel Investigation at a Mach Number of 2.01 of the Sonic-Boom Characteristics of Three Wing-Body Combinations Differing in Wing Longitudinal Location. NASA TN D-1384, 1962.

8. Mullens, Marshall E.: A Flight Test Investigation of the Sonic Boom. AFFTC-TN-56-20, Air Res. and Dev. Command, U.S. Air Force, May 1956.

9. Maglieri, Domenic J.; Hubbard, Harvey H.; and Lansing, Donald L.: Ground Measurements of the Shock-Wave Noise From Airplanes in Level Flight at Mach Numbers to 1.4 and at Altitudes to 45,000 Feet. NASA TN D-48, 1959.

10. Lina, Lindsay J.; and Maglieri, Domenic J.: Ground Measurements of Airplane Shock-Wave Noise at Mach Numbers to 2.0 and at Altitudes to 60,000 Feet. NASA TN D-235, 1960.

11. Maglieri, Domenic J.; and Hubbard, Harvey H.: Ground Measurements of the Shock-Wave Noise From Supersonic Bomber Airplanes in the Altitude Range From 30,000 to 50,000 Feet. NASA TN D-880, 1961.

12. Hubbard, Harvey H.; Maglieri, Domenic J.; Huckel, Vera; and Hilton, David A. (With appendix by Harry W. Carlson): Ground Measurements of Sonic-Boom Pressures for the Altitude Range of 10,000 to 75,000 Feet. NASA TR R-198, 1964. (Supersedes NASA TM X-633.)

13. Maglieri, Domenic J.; Ritchie, Virgil S.; and Bryant, John F., Jr.: In-Flight Shock-Wave Pressure Measurements Above and Below a Bomber Airplane at Mach Numbers From 1.42 to 1.69. NASA TN D-1968, 1963.

14. Rao, P. Sambasiva: Supersonic Bangs - Part 1. Aero. Quarterly, vol. VII, pt. I, Feb. 1956, pp. 21-44.

15. Rao, P. Sambasiva: Supersonic Bangs - Part 2. Aero. Quarterly, vol. VII, pt. II, May 1956, pp. 135-155.

16. Lansing, Donald L.: Some Effects of Flight Path Upon the Distribution of Sonic Booms. Proc. Symposium on Atmospheric Acoustic Propagation, vol. I, June 14-16, 1961, pp. 24-43. (Sponsored by U.S. Army Signal Missile Support Agency and Texas Western College.)

17. Barger, Raymond L.: Some Effects of Flight Path and Atmospheric Variations on the Boom Propagated From a Supersonic Aircraft. NASA TR R-191, 1964.

18. Friedman, Manfred P.; Kane, Edward J.; and Sigalla, Armand: Effects of Atmosphere and Aircraft Motion on the Location and Intensity of a Sonic Boom. AIAA Jour., vol. 1, no. 6, June 1963, pp. 1327-1335.

19. Kerr, T. H.: Experience of Supersonic Flying Over Land in the United Kingdom. Rep. 250, AGARD, North Atlantic Treaty Organization (Paris), Sept. 1959.

20. Maglieri, Domenic J.; and Lansing, Donald L.: Sonic Booms From Aircraft in Maneuvers. NASA TN D-2370, 1964.

21. Maglieri, Domenic J.; and Parrott, Tony L.: Atmospheric Effects on Sonic-Boom Pressure Signatures. Sound, vol. 2, no. 4, July-Aug. 1963, pp. 11-14.

22. Cawthorn, Jimmy M.: Some Sonic-Boom Induced Building Responses. Paper Presented at Sixty-Sixth Meeting of Acoustical Soc. of America (Ann Arbor, Mich.), Nov. 1963.

23. Maglieri, Domenic J.; Huckel, Vera; and Parrott, Tony L.: Ground Measurements of Shock-Wave Pressure for Fighter Airplanes Flying at Very Low Altitudes and Comments on Associated Response Phenomena. NASA TM X-611, 1961.

24. Power, J. K.; and Bates, George: Sonic Boom & Community Relations. [Preprint] 683B, Soc. Automotive Eng., Apr. 1963.

25. Jones, L. B.: Lower Bounds for Sonic Bangs. Jour. R.A.S. (Tech. Notes), vol. 65, no. 606, June 1961, pp. 433-436.

26. Carlson, Harry W.: The Lower Bound of Attainable Sonic-Boom Overpressure and Design Methods of Approaching This Limit. NASA TN D-1494, 1962.

27. Carlson, Harry W.: Influence of Airplane Configuration on Sonic-Boom Characteristics. NASA RP-208, 1964. (Reprinted from J. Aircraft, vol. 1, no. 2, Mar.-Apr. 1964, pp. 82-86.)

"The aeronautical and space activities of the United States shall be conducted so as to contribute . . . to the expansion of human knowledge of phenomena in the atmosphere and space. The Administration shall provide for the widest practicable and appropriate dissemination of information concerning its activities and the results thereof."

—NATIONAL AERONAUTICS AND SPACE ACT OF 1958

NASA SCIENTIFIC AND TECHNICAL PUBLICATIONS

TECHNICAL REPORTS: Scientific and technical information considered important, complete, and a lasting contribution to existing knowledge.

TECHNICAL NOTES: Information less broad in scope but nevertheless of importance as a contribution to existing knowledge.

TECHNICAL MEMORANDUMS: Information receiving limited distribution because of preliminary data, security classification, or other reasons.

CONTRACTOR REPORTS: Technical information generated in connection with a NASA contract or grant and released under NASA auspices.

TECHNICAL TRANSLATIONS: Information published in a foreign language considered to merit NASA distribution in English.

TECHNICAL REPRINTS: Information derived from NASA activities and initially published in the form of journal articles.

SPECIAL PUBLICATIONS: Information derived from or of value to NASA activities but not necessarily reporting the results of individual NASA-programmed scientific efforts. Publications include conference proceedings, monographs, data compilations, handbooks, sourcebooks, and special bibliographies.

Details on the availability of these publications may be obtained from:

SCIENTIFIC AND TECHNICAL INFORMATION DIVISION

NATIONAL AERONAUTICS AND SPACE ADMINISTRATION

Washington, D.C. 20546